P H Y S I C A L   R E V I E W   L E T T E R S

Coherent Spin Transport through a 350 Micron Thick Silicon Wafer

Biqin Huang,[1,*] Douwe J. Monsma,[2] and Ian Appelbaum[1]

[1]*Electrical and Computer Engineering Department, University of Delaware, Newark, Delaware, 19716, USA*
[2]*Cambridge NanoTech Inc., Cambridge, Massachusetts 02139, USA*

We use all-electrical methods to inject, transport, and detect spin-polarized electrons vertically through a 350-micron-thick undoped single-crystal silicon wafer. Spin precession measurements in a perpendicular magnetic field at different accelerating electric fields reveal high spin coherence with at least 13π precession angles. The magnetic-field spacing of precession extrema are used to determine the injector-to-detector electron transit time. These transit time values are associated with output magnetocurrent changes (from in-plane spin-valve measurements), which are proportional to final spin polarization. Fitting the results to a simple exponential spin-decay model yields a conduction electron spin lifetime (T_1) lower bound in silicon of over 500 ns at 60 K.

Silicon (Si) has been broadly viewed as the ideal material for spintronics due to its low atomic weight, lattice inversion symmetry, and low isotopic abundance of species having nuclear spin [1–3]. These qualities are in contrast to the high atomic weight, inversion-asymmetric zinc blende lattice, and high nuclear spin of the well-studied semiconductor GaAs [4–10], which consequently has a relatively large spin-orbit and hyperfine interaction [1]. The resulting long spin lifetime and spin coherence lengths in Si may therefore enable spin-based Si integrated circuits [11,12].

Despite this appeal, however, the experimental difficulties of achieving coherent spin transport in silicon were first overcome only recently, by using unique spin-polarized hot-electron injection and detection techniques [13–16]. (Subsequently, tunnel spin injection was demonstrated using optical detection with circular polarization analysis of weak indirect-bandgap electroluminescence [17].) In Refs. [13,14], spin transport through 10 μm of silicon was demonstrated and a spin lifetime lower bound of ≈ 1 ns at 85 K was estimated. Using a new type of hot-electron spin injector that gives higher spin polarization and output current, we now show that (as with all-optical methods at 1.6 K in GaAs) [5] coherent spin transport can be observed over much longer length scales: we demonstrate transport vertically through a 350 μm-thick silicon wafer, and derive a spin lifetime of at least 500 ns at 60 K (2 orders of magnitude higher than metals or other semiconductors such as GaAs at similar temperature [4,18]).

As in Refs. [13–16], we use ultrahigh vacuum metal-film wafer bonding [19] to build a semiconductor-metal-semiconductor hot-electron spin detection structure. A $2''$ diameter double-side polished 350-micron-thick undoped (resistivity >13 k$\Omega \cdot$cm @ room-temperature) single-crystal Si(100) wafer is bonded to a 1–10 $\Omega \cdot$cm n-type Si(100) wafer with a 4 nm $Ni_{80}Fe_{20}$/4 nm Cu bilayer [19,20]. (The Cu layer is necessary to reduce the hot-electron collector Schottky barrier height [21].) During thermal evaporation of 2 nm $Ni_{80}Fe_{20}$ on both wafers, the ultraclean surfaces of the deposited metal films were

pressed together *in situ* with nominal force, forming a cohesive bond with a recrystallized 4 nm-thick $Ni_{80}Fe_{20}$ layer [19].

Although these bonding steps are identical to our previous reports with 10 μm-thick transport layer devices, the subsequent procedure used to fabricate 350 μm-thick transport layer devices differs significantly. In the present work, the outside polished surface of the undoped Si wafer in the bonded pair was covered by a protective 1 μm-thick SiO_2 layer deposited by an electron-beam source. A wafer saw was used to first cut through the undoped Si wafer and buried metal bonding layer, partially through the n-Si wafer to define individual device mesas. Then, the saw was used to cut trenches in the undoped Si wafer close to, but not through, the buried metal bilayer. Wet chemical etching with tetramethyl ammonium hydroxide (TMAH) removed the remaining Si and exposed the buried $Ni_{80}Fe_{20}$ for electrical contact [22]. After protective SiO_2 removal with buffered HF, a 40 nm Al/10 nm $Co_{84}Fe_{16}$/Al_2O_3/5 nm Al/5 nm Cu tunnel junction hot-electron spin injector was deposited using electron-beam evaporation through shadow masks for lateral patterning [16].
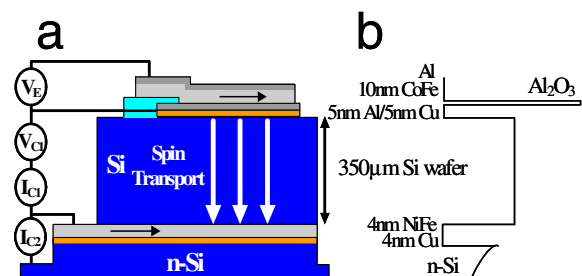

FIG. 1 (color online). (a) Schematic side view with electrical configuration shown, and (b) associated conduction-band diagram and constituent layers of the Si spin-transport device. Spin-polarized electrons are injected from the top of the device and drift in an electric field to the bottom where they are detected with a semiconductor-ferromagnetic metal-semiconductor structure employing spin-dependent hot-electron scattering.

The schematic side view and associated conduction-band diagram in Figs. 1(a) and 1(b), respectively, show the vertical geometry of our four-terminal Si spin transport devices and can be used to elucidate the means of spin injection and detection. When a voltage bias V_E is applied across the emitter tunnel junction, electrons that are spin polarized at the cathode $Co_{84}Fe_{16}/Al_2O_3$ interface tunnel through the oxide barrier and some travel ballistically through the nonmagnetic Al/Cu anode bilayer. Those electrons with energy above the Cu/Si Schottky barrier (≈ 0.6 eV) [23] can couple with Si conduction-band states and then quickly thermalize to the conduction-band minimum [24]. These spin-polarized electrons are then accelerated in an applied electric field vertically through the 350 μm-thick wafer and toward the opposite side of the undoped Si, where they are ejected from the conduction band into the buried metal layer. Because the ferromagnetic $Ni_{80}Fe_{20}$ layer has a spin-dependent band structure, the inelastic scattering rates of these hot electrons to the Fermi energy is also spin dependent. Therefore, the number of ballistic electrons that can couple with conduction-band states in the n-Si collector on the other side (forming the "second collector current" I_{C2}) is dependent on the relative orientation of final spin direction and ferromagnet (FM) magnetization.

The spin-polarized electron injector we use here is notably different from the design in previous studies, where spin-dependent scattering in the base anode (ballistic spin filtering) was the operating mechanism [13–15]. In the devices used in the present work, initial spin polarization is obtained by direct tunneling from the cathode FM ($Co_{84}Fe_{16}$) through the Al_2O_3 tunnel junction oxide. This design gives several advantages. (i) The FM is removed from the Si surface, preventing the formation of a nonmagnetic silicide having strong, randomly-oriented magnetic moments. The elimination of this "magnetically-dead" region (which could cause significant spin scattering) maintains a high initial spin polarization [16]. (ii) Ballistic hot-electron transport before injection into the Si conduction band is through nonmagnetic Al and Cu, which have much larger ballistic mean-free paths than typical FMs, resulting in higher injected current (I_{C1}) and the spin-signal output current (I_{C2}) it drives. (iii) The Cu/Si Schottky barrier height is relatively low [23], further increasing I_{C1}.

If spin "up" is both injected and detected with parallel FM magnetizations (and no spin flipping or rotating process occurs in the Si bulk) a relatively high I_{C2} should be measured. On the other hand, if spin up is injected, but spin "down" is detected (with antiparallel FM magnetizations), I_{C2} will be relatively lower, again assuming no spin flips or rotations. The ferromagnetic layers chosen for the injector ($Co_{84}Fe_{16}$) and detector ($Ni_{80}Fe_{20}$) have different coercive (or switching) fields, which enables external control over the relative orientation of spin injection and detection axes with an in-plane magnetic field. At 150 K, clean spin-valve signals at constant emitter bias $V_E = -1.3$ V and accel-

erating voltage $V_{C1} = 20$ V (resulting in ≈ 580 V/cm electric field) [14] indicate a $\approx 18\%$ change in I_{C2} when the magnetizations of injector and detector are switched from a parallel (P) to antiparallel (AP) configuration by an externally applied in-plane magnetic field, according to our expectations (as shown in Fig. 2). This magnetocurrent ratio (MC $= (I_{C2}^P - I_{C2}^{AP})/I_{C2}^{AP}$) corresponds to an electron current spin polarization of approximately $\mathcal{P} =$ MC/(MC + 2) $\approx 8\%$ [15]. However, this evidence for spin transport is not conclusive without observation of spin precession and dephasing (Hanle effect [25,26]) in a perpendicular magnetic field [27].

A perpendicular magnetic field $\vec{B}$ exerts a torque $(g\mu_B/\hbar)\vec{S} \times \vec{B}$ on the electron spin $\vec{S}$, causing spin rotation (precession) about $\vec{B}$. Here, g is the electron spin g factor, μ_B is the Bohr magneton, and $\hbar$ is the reduced Planck constant. Our spin detector measures the projection of final spin angle on an axis determined by the $Ni_{80}Fe_{20}$ magnetization, so we observe oscillations in I_{C2} as the precession frequency $\omega = g\mu_B B/\hbar$ is varied.

Figure 3(a) shows our measurement of I_{C2} in varying perpendicular magnetic field with the same temperature and bias conditions as in Fig. 2. The measurement begins at negative field values when the injector or detector magnetizations are in a parallel orientation. As the field is increased, we see multiple oscillations due to spin precession. However, when the field reaches $\approx +38$ Oe, a small in-plane component of the applied field switches the magnetization of the magnetically softer $Ni_{80}Fe_{20}$, resulting in an antiparallel injector and detector orientation that inverts the magnitudes of maxima and minima.

The final precession angle θ at the detector is simply the product of transit time from injector-to-detector, τ, and spin precession frequency ω. Since our measurement is an average of the precession angles over all electrons arriving at the detector regardless of transit time τ, the magnitudes of higher-order extrema [labeled in Fig. 3(a)]
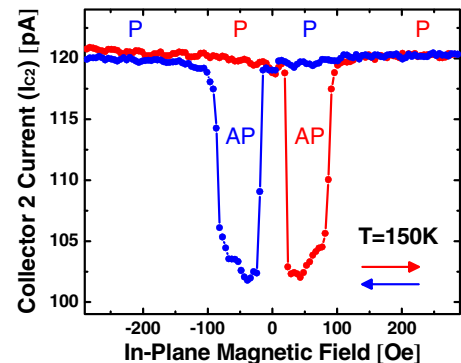

FIG. 2 (color online).   In-plane magnetic hysteresis measurement of second collector current I_{C2} at constant emitter voltage bias $V_E = -1.3$ V and constant accelerating voltage $V_{C1} = 20$ V, showing $\approx 18\%$ spin-valve effect at 150 K. The labels "P" and "AP" refer to parallel and antiparallel injector and detector magnetization configuration, respectively. Injected current I_{C1} is 6.6 μA.
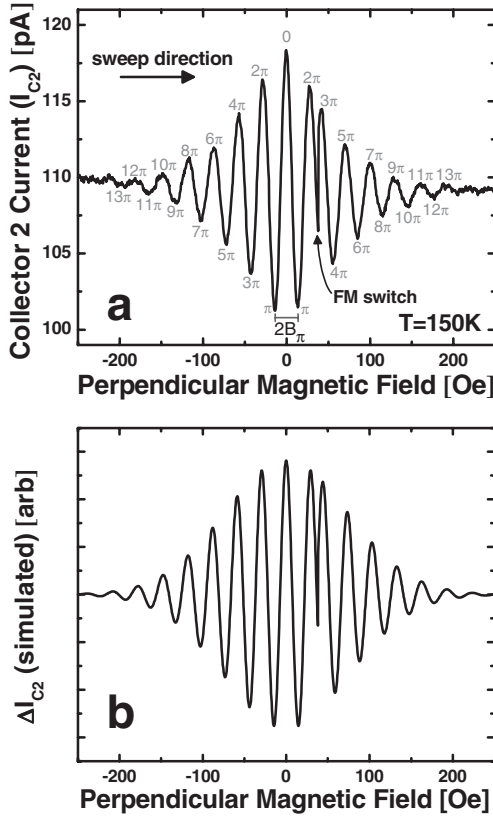
FIG. 3.   (a) Spin precession and dephasing (Hanle effect) of Si conduction-band electrons in a perpendicular magnetic field at 150 K using the same voltage bias conditions as in Fig. 2, showing up to 13π rad precession angles. The "FM switch" is caused by a residual in-plane magnetic field component switching the in-plane magnetization of the Ni$_{80}$Fe$_{20}$ detector at $\approx$ +38 Oe, which inverts the maxima and minima at higher positive field values. (b) Simulation of the measurement in (a), using the drift-diffusion spin precession model given by Eq. (1).

are reduced by the dephasing associated with a distribution in transit times $\Delta\tau$ caused by random diffusion.

We can simulate our measurement in the presence of both drift and diffusion by integrating the contributions to our signal from an ensemble of precessing spins with a diffusion-controlled distribution of transit times using a simple model [7,28]:

$$\Delta I_{C2} \sim \int_0^\infty \frac{1}{2\sqrt{\pi Dt}} e^{-[(x-vt)^2/4Dt]} \cos(\omega t) e^{-t/\tau_{sf}} dt, \quad (1)$$

where D is the diffusion constant, v is drift velocity, and τ_{sf} is effective spin lifetime. The integrand is simply the product of the effects of drift and diffusion, precession, and finite spin lifetime. Using $x = L = 350$ μm, $D = 200$ cm^2/s, $v = 2.9 \times 10^6$ cm/s [29], and $\tau_{sf} = 73$ ns (see below), we find excellent agreement between experiment and model in Fig. 3(b). (In this simulation, the sign is inverted for magnetic field values >38 Oe to match the experimental results.)

Despite transport through 350 microns of undoped Si, high spin coherence with at least 13π spin precession angle (more than six full rotations) is evident in Fig. 3(a), which is even greater than what was previously demonstrated using a much shorter 10 μm-thick transport layer [13]. Because the transit time is therefore much longer in the thicker devices, it could be argued that diffusion should play a larger role and dephasing should suppress multiple oscillations in precession measurements. The results of the experiment and consistent model simulation clearly conflict with this reasoning.

The somewhat counterintuitive result can be explained with a simple argument: If transport is dominated by drift in the applied electric field [14], the transit time is given by $\tau = L/v = L^2/(\mu V_{C1})$, where μ is the electron mobility, L is the transport length, and v is drift velocity [28]. The width d of an initially injected infinitesimally-narrow Gaussian spin distribution will increase by diffusion during this transit time to $d = \sqrt{D\tau} = L\sqrt{D/(\mu V_{C1})}$. Since the width of the distribution of transit times $\Delta\tau$ is d/v, the relative uncertainty in the distribution of final precession angle θ at the detector is $\Delta\theta/\theta = \frac{\omega \cdot \Delta\tau}{\omega\tau} = \sqrt{D/(\mu V_{C1})}$. This result is independent of the transit length L, so we can expect the same amount of dephasing regardless of the distance from injector to detector for any fixed precession angle and accelerating voltage (assuming Ohmic behavior, $v = \mu E$, where E is the internal electric field).

From the oscillation period of spin precession measurements [$2B_\pi$, as shown in Fig. 3(a)], we can determine the average spin transit time in any given accelerating electric drift field conditions (induced by V_{C1}) through $\tau = h/(2g\mu_B B_\pi)$. The normalized magnetocurrent $\Delta I_{C2}/I_{C1}$ determined by spin-valve measurements like those in Fig. 2 gives a quantity that is proportional to conduction electron current spin polarization, $\mathcal{P}$ [13,14]. Associating this value with the transit times given by precession measurements (see above) gives data which can be fit with a simple exponential decay model, where

$$\mathcal{P} \propto \exp(-\tau/T_1). \quad (2)$$

The time scale T_1 is the longitudinal spin lifetime, since our spin-polarization data is derived from spin-valve measurements with in-plane magnetic fields colinear to the spin direction.

The best-fits to our data at 60, 85, 100, 125, and 150 K using the expression in Eq. (2) are 520, 269, 201, 96, and 73 ns, respectively, as shown in Figs. 4(a) and 4(b). These lifetimes are much greater than the $\approx$1 ns lifetime lower bound estimated in previous work, because with the much longer transit lengths here, the applied accelerating voltage V_{C1} varies the transit time over a range of $\approx$200 ns; previously the range was only several hundred ps, and parasitic electronic effects suppressed our estimate [13,14]. The temperature dependence of these spin lifetimes fit well to the expected behavior in an indirect-bandgap semiconductor predicted by Yafet ($\propto T^{-5/2}$), as shown in
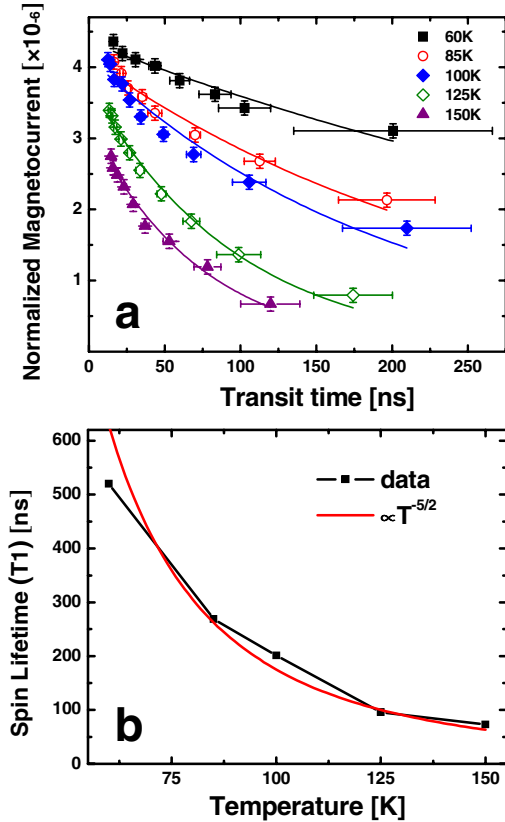
PHYSICAL REVIEW LETTERS

FIG. 4 (color online). (a) Fitting the normalized magnetocurrent ratio ($\Delta I_{C2}/I_{C1}$) to an exponential decay model (Eq. (2)) using transit times derived from spin precession measurements (like those in Fig. 3(a)) at variable internal electric field yields measurement of longitudinal spin lifetimes (T_1) in undoped bulk Si. (b) The experimental T_1 values obtained as a function of temperature are compared to Yafet's $T^{-5/2}$ power law for indirect-bandgap semiconductors [30].

Fig. 4(b) [30–32]. The relative absence of other relaxation mechanisms in Si is responsible for the long spin lifetimes.

Certainly, higher temperature operation is desirable. However, thermionic leakage at the second collector Schottky barrier and the difficulties of reliably operating our tunnel junction spin injector at high voltages necessary are the present limitation to increasing this temperature. Although observation of spin precession at high electric fields are possible at lower temperatures, measurements of spin lifetime below 60 K are currently prevented by carrier freeze-out effects.

The long lifetimes measured here are lower bounds, with the possibility that parasitic electronic effects artificially suppress the values obtained [14]. Hence, spin lifetimes could be higher with associated longer transport lengths. Because of the thickness limitations of Si wafers, we will explore these longer distances with lateral transport devices. This achievement should enable true spintronic circuits intimately compatible with existing Si based logic, and potentially extend the performance trend of Si devices beyond its limits set by conventional approaches.

*bqhuang@udel.edu
[1] I. Žutić, J. Fabian, and S. Das Sarma, Rev. Mod. Phys. **76,** 323 (2004).
[2] I. Žutić, J. Fabian, and S. C. Erwin, Phys. Rev. Lett. **97,** 026602 (2006).
[3] A. M. Tyryshkin, S. A. Lyon, A. V. Astashkin, and A. M. Raitsimring, Phys. Rev. B **68,** 193207 (2003).
[4] J. M. Kikkawa and D. D. Awschalom, Phys. Rev. Lett. **80,** 4313 (1998).
[5] J. M. Kikkawa and D. D. Awschalom, Nature (London) **397,** 139 (1999).
[6] X. Lou *et al.*, Phys. Rev. Lett. **96,** 176603 (2006).
[7] X. Lou *et al.*, Nature Phys. **3,** 197 (2007).
[8] X. Jiang *et al.*, Phys. Rev. Lett. **90,** 256603 (2003).
[9] X. Jiang *et al.*, Phys. Rev. Lett. **94,** 056601 (2005).
[10] M. Holub, J. Shin, D. Saha, and P. Bhattacharya, Phys. Rev. Lett. **98,** 146603 (2007).
[11] I. Žutić and J. Fabian, Nature (London) **447,** 269 (2007).
[12] M. A. Nielsen and I. L. Chuang, *Quantum Computation and Quantum Information* (Cambridge University Press, Cambridge, England, 2000).
[13] I. Appelbaum, B. Huang, and D. Monsma, Nature (London) **447,** 295 (2007).
[14] B. Huang, D. Monsma, and I. Appelbaum, J. Appl. Phys. **102,** 013901 (2007).
[15] B. Huang, D. Monsma, and I. Appelbaum, Appl. Phys. Lett. **91,** 072501 (2007).
[16] B. Huang, L. Zhao, D. Monsma, and I. Appelbaum, Appl. Phys. Lett. **91,** 052501 (2007).
[17] B. T. Jonker *et al.*, Nature Phys. **3,** 542 (2007).
[18] D. D. Awschalom, D. Loss, and N. Samarth, *Semiconductor Spintronics and Quantum Computation* (Springer, New York, 2004).
[19] D. J. Monsma, R. Vlutters, and J. C. Lodder, Science **281,** 407 (1998).
[20] R. Jansen, J. Phys. D **36,** R289 (2003).
[21] D. J. Monsma, J. C. Lodder, Th. J. A. Popma, and B. Dieny, Phys. Rev. Lett. **74,** 5260 (1995).
[22] B. Huang, I. Altfeder, and I. Appelbaum, Appl. Phys. Lett. **90,** 052503 (2007).
[23] S. Sze, *Physics of Semiconductor Devices* (Wiley, New York, 1981), 2nd ed..
[24] L. D. Bell *et al.*, Phys. Rev. B **48,** 5712 (1993).
[25] M. Johnson and R. H. Silsbee, Phys. Rev. B **37,** 5326 (1988).
[26] M. Johnson and R. H. Silsbee, Phys. Rev. Lett. **55,** 1790 (1985).
[27] F. G. Monzon, H. X. Tang, and M. L. Roukes, Phys. Rev. Lett. **84,** 5022 (2000).
[28] I. Appelbaum and D. J. Monsma, Appl. Phys. Lett. **90,** 262501 (2007).
[29] C. Canali *et al.*, Phys. Rev. B **12,** 2265 (1975).
[30] Y. Yafet, in *Solid State Physics*, edited by F. Seitz and D. Turnbull (Academic, New York, 1963), Vol. 14.
[31] D. J. Lepine, Phys. Rev. B **2,** 2429 (1970).
[32] J. Fabian *et al.*, Acta Phys. Slovaca **57,** 565 (2007).